PPPL-2502

PPPL-2502

UC-426,427

SOFT X-RAY AMPLIFICATION IN LITHIUM-LIKE AL XI (154 Å) AND SI XII (129 Å)

By

D. Kim, C.H. Skinner, A. Wouters,
E. Valeo, D. Voorhees, and S. Suckewer

MARCH 1988

PLASMA PHYSICS LABORATORY

PRINCETON UNIVERSITY
PRINCETON, NEW JERSEY

PREPARED FOR THE U.S. DEPARTMENT OF ENERGY,
UNDER CONTRACT DE-AC02-76-CHO-3073.

NOTICE

Printed in the United States of America

Available from:

National Technical Information Service
U.S. Department of Commerce
5285 Port Royal Road
Springfield, Virginia 22161

Price Printed Copy $__*__; Microfiche $4.50

*Pages	NTIS Selling Price
1-25	$7.00
25-50	$8.50
51-75	$10.00
76-100	$11.50
101-125	$13.00
126-150	$14.50
151-175	$16.00
176-200	$17.50
201-225	$19.00
226-250	$20.50
251-275	$22.00
276-300	$23.50
301-325	$25.00
326-350	$26.50
351-375	$28.00
376-400	$29.50
401-425	$31.00
426-450	$32.50
451-475	$34.00
476-500	$35.50
500-525	$37.00
526-550	$38.50
551-575	$40.00
567-600	$41.50

For documents over 600 pages, add $1.50 for each additional 25-page increment.

PPPL--2502

DE88 00933o

SOFT X-RAY AMPLIFICATION IN LITHIUM-LIKE AL XI (154 Å) AND SI XII(129 Å)

D. Kim, C. H. Skinner, A. Wouters,

E. Valeo, D. Voorhees, and S. Suckewer*

Plasma Physics Laboratory, Princeton University

Princeton, NJ 08544

Abstract

Recent experiments on soft x-ray amplification in lithium-like ions in a CO_2 laser-produced recombining plasma confined in a magnetic field are presented. The maximum gain-length products observed are GL $\simeq$ 3-4 for the 154 Å, 4f-3d transition in Al XI and GL $\simeq$ 1-2 for the 129 Å, 4f-3d transition in Si XII, respectively. A one-dimensional hydrodynamic code with a collisional-radiative atomic model was used to model the plasma and the theoretical predictions of gain agree well with the observations. Descriptions of both hydrodynamic and atomic physics code are given.

I. Introduction

Since the demonstration of high amplification of soft x-rays in laser-produced plasmas,[1,2] different approaches to improve x-ray laser characteristics to shorter wavelengths, higher power, better coherence, narrower divergence, and better efficiency are being pursued at several laboratories.[3-11] In terms of improving the power, coherence, and divergence, we have developed an experimental system with which a series of experiments on soft x-ray laser cavities will be performed. An x-ray laser operating wavelength between K-edge of carbon at 44 Å and that of oxygen at 25 Å would be optimal in terms of penetration, contrast, and resolution for microscopy of biological specimens. At Princeton we are working to make a shorter wavelength soft x-ray laser using two approaches. One approach is to produce a population inversion in Kr-like or Ar-like ions through selective excitation by multiphoton transitions[12] or inner-shell ionizations. The inner-shell ionization scheme was proposed initially by Duguay and Rentzepis,[13] modified later by McGuire,[14] and recently demonstrated experimentally at 1089 Å.[8,9] In our approach, the plasma of the desired ionization stage will be produced by a CO_2 or Nd-glass laser and then, via multiphoton transitions or inner-shell ionizations, will be excited by a powerful picosecond laser. The instrumentation for this approach has been developed and a series of experiments is planned in the near future. The subject of this paper is an approach based on a recombination scheme using magnetically confined ($\leq$ 100 kG) lithium-like ions produced by a $\sim$ 500 J, 50-70 ns CO_2 laser. This scheme has been successfully used to make a soft x-ray laser in hydrogen-like C VI with the following characteristics:

182 A wavelength, 500 amplification, 1-3 mJ pulse energy, 10-30 ns pulse duration, and 5 mrad beam divergence.[6]

An extensive series of experiments for developing a soft x-ray laser using lithium-like ions has been performed by Jaeglé et al.[5] In these experiments a Nd laser produces a freely expanding plasma, generating a population inversion between 5f and 3d levels in Li-like Al XI, and a gain-length product of 2-2.5 between those levels has been reported. More recently, Jaeglé and his group in experiments in collaboration with the Rutherford Appleton Laboratory measured gain also for 4f-3d transition in Li-like Al XI, using a carbon fiber coated with a thin layer of Al.[15] At Princeton early investigations of lithium-like spectra have showed also evidence of population inversions between the 3d and 4f levels in O VI and Ne VIII[16,17] with an estimated gain of 1.8 cm^{-1} for the case of O VI.

In the recombination scheme, a powerful laser is focused onto a solid target, creating large population of ions in an ionization stage, above the one in which a population inversion between excited levels is desired, i.e., He-like ions for a population inversion in Li-like ions. Then, rapid cooling after the laser pulse by radiation (impurities are added to increase the radiative cooling) and the maintenance of high electron density of $n_e \sim 5 \times 10^{18}$ cm^{-3} by the magnetic field make favorable conditions for a population inversion between two low-lying excited levels such as 4f and 3d levels in Li-like ions. At a relatively low electron temperature and high electron density, three-body recombination followed by cascading processes dominates collisional ionization and excitation processes, populating the upper level (4f) while the lower level (3d) decays

rapidly by its strong radiative transition. In this way, a population inversion between two excited levels is created.

An important feature in Li-like ions is the fast radiative transition of the 3d level to 2p due to the large overlap of the radial wavefunctions of those levels, so that the 3d level is rapidly depopulated during the recombination phase, permitting a population inversion to be built up. Another merit of Li-like ions is a lower ionization potential than H-like ions with a comparable lasing wavelength. For example, Si XII has an ionization potential of 523 eV for a 4f-3d transition at 129 Å, compared to H-like N VII has an ionization potential of 667 eV for a 3-2 transition at 134 Å. However, for a given plasma electron density, such as may be limited to approximately 1×10^{19} cm^{-3}, which is the critical density for the CO_2 laser, the ion density of Si XII is lower than that of N VII. The trade-off between these and other factors is a subject of theoretical and experimental investigations.

In section II we discuss the main features of the one-dimensional Lagrangian hydrodynamic code and the atomic physics code applied to modeling of time development of the gain in the recombining Li-like plasma. In section III the experimental set-up and results are presented and compared with theoretical calculations.

II. Theoretical model

A. Hydrodynamic model

In this section we discuss the basic features of the one-dimensional hydrodynamic model[18] which was developed to provide insight into the behavior of the magnetically

confined, laser-produced carbon plasma used in the 182 Å soft x-ray laser. One of the first hydrodynamic computer codes was developed in NRL and used to study the laser-produced plasmas.[19] A more detailed description of this model will be published elsewhere. The hydrodynamic code with atomic data on the experimental species (in our case Al or Si) and the atomic physics code (discussed below) for Li-like ions enabled us to simulate experiments with Li-like ions.

The basic equations to be solved for a cylindrical plasma are presented below:

The continuity equation is given by:

$$\frac{\partial n_i}{\partial t} + \frac{1}{r}\frac{\partial}{\partial r}(r n_i v) = \delta_i - \frac{1}{r}\frac{\partial}{\partial r}(Dr\frac{\partial n_i}{\partial r}), \tag{1}$$

where n_i is a population of the ground state of the i-th ionization stage, v the mean fluid velocity, and δ_i is given by

$$\delta_i = -n_e n_i R_i - n_e n_i S_i + n_e n_{i+1} R_{i-1} + n_e n_{i-1} S_{i-1},$$

where S_i is the collisional ionization rate from the ground state of the i-th ionization stage,[20] and R_i represents the collisional dielectronic recombination coefficient of Summers.[21,22] Summers has calculated this coefficient, taking into account recombinations to and ionizations from excited and ground states. Recombination to and ionization from neutrals are neglected because we are interested in a high ionization stage, e.g., Al^{+10}. The second term in the right-hand side of Eq.(1) takes into account the ion-ion diffusion process. The transport of He-like Al XII from the central laser-heated region to the off-axis, cold region where they recombine into Li-like ions is crucial to the generation of high gain. Figure 1 shows the variation of the maximum gain for the 4f-3d transition in Li-like Al XI and the radial position where

the maximum gain occurs with different values of the diffusion coefficient. This was generated with the laser input energy kept constant. D = 5×10^3 cm^2/sec was chosen throughout calculations because it produces the highest gain at the proper position observed experimentally.[2] This value is several orders of magnitude higher than the classical diffusion coefficient at $T_i \simeq 100$ eV and $n_e \simeq 1 \times 10^{18}$ cm^{-3}. To understand this discrepancy requires an investigation of diffusion processes in the laser-produced, dense plasma, which is beyond the scope of the present paper.

The equation of motion is :

$$Mn(\frac{\partial v}{\partial t} + v\frac{\partial v}{\partial r}) + \frac{\partial}{\partial r}(k[n_eT_e + nT_i] + Q) = -\frac{B}{4\pi}\frac{\partial B}{\partial r}, \qquad (2)$$

where M is the ion mass, n total ion density, $n = \sum_i n_i$, k the Boltzmann constant, T_e and T_i electron and ion temperature, respectively, and B the magnetic field strength. Q denotes the artificial viscosity term to handle the shock wave due to the strong expansion.[23]

$$Q = AMn(\frac{\partial v}{\partial r})^2 \quad \text{if} \quad \frac{\partial v}{\partial r} < 0,$$
$$0 \quad \text{if} \quad \frac{\partial v}{\partial r} > 0,$$

where A is a constant, chosen in such a way that no numerical instabilities take place due to the propagation of a shock wave.

Laser radiation is absorbed by electrons and electrons exchange their energy with ions at the classical equipartition rate. It is assumed that the shock wave heats ions only and the electrons behave adiabatically. Then, the electron temperature is given

by:

$$\frac{\partial T_e}{\partial t} + v\frac{\partial T_e}{\partial r} = -\frac{2}{3}T_e\frac{1}{r}\frac{\partial}{\partial r}(rv) - \frac{2}{3n_e}\frac{1}{r}\frac{\partial}{\partial r}(\kappa_e r\frac{\partial T_e}{\partial r}) + \frac{2}{3n_e}\epsilon_J - \frac{T_e - T_i}{\tau_{eq}} + \frac{2}{3n_e}\epsilon_L - \frac{2}{3}P_{atom}. \quad (3)$$

where κ_e is the electron thermal conductivity divided by the Boltzmann constant k, and terms in the right-hand side represent work done on expansion, thermal conduction losses, ohmic heating due to the induced current, energy transfer to ions, laser energy input, successively, and the last term is energy losses by atomic processes:

$$P_{atom} = P_{rad} + P_{ionization} - P_{recombination} + P_{impurity},$$

where P_{rad} denotes the total energy loss by resonant radiations following collisional excitations, $P_{ionization}$ the total energy loss by ionization processes, $P_{recombination}$ the total energy recovery by recombination processes, and $P_{impurity}$ the total energy loss by an impurity (iron in our calculation). The ohmic heating term is defined by the plasma resistivity η as $\epsilon_J = [c^2\eta/(4\pi)^2](\partial B/\partial r)^2$. c is the speed of light. τ_{eq} in Eq.(3) is the energy equilibration time between electrons and ions and ϵ_L is the power per unit volume absorbed by electrons from the laser. Impurities are assumed to be distributed uniformly. Data for the electron cooling rate of iron in a dense, transient plasma are not available. As a first approximation we have used the radiation cooling rates of Post et al.[24] for a steady-state, coronal plasma. At high electron densities, the radiation cooling coefficient per electron per ion is reduced due to the decrease of energy loss through $\Delta n = 0$ transitions as a result of the increase of collisional de-excitation rates.[25] Figure 2 shows the reduction factor of the radiation cooling coefficient per electron per ion, $1 + n_e S_{lm}^{II}/A_{lm}$, versus the electron temperature for

$\Delta n = 0$ transitions in iron at given electron densities. S_{lm}^{II} and A_{lm} are collisional de-excitation and radiative transition rates, weight-averaged over the possible allowed $\Delta n = 0$ transitions. Expressions by Post et al.[24] in an average-ion model were used for S_{lm}^{II} and A_{lm}. At the condition of $T_e = 5$ eV and $n_e \simeq 4 \times 10^{18}$cm^{-3}, the radiation cooling rate of Post et al. would be reduced by about one order of magnitude. More complete calculation of the cooling rate by iron in the high electron densities above the coronal limit is planned using an average-ion model. Results with the present code, however, are in a reasonable agreement with experimental data, as is discussed in section III.

The ion temperature is governed by:

$$\frac{\partial T_i}{\partial t} + v\frac{\partial T_i}{\partial r} = -\frac{2}{3}(T_i + \frac{Q}{n})\frac{1}{r}\frac{\partial}{\partial r}(rv) + \frac{2}{3}\frac{1}{n}\frac{1}{r}\frac{\partial}{\partial r}(\kappa_i r\frac{\partial T_i}{\partial r}) + \frac{T_e - T_i}{\tau_{eq}}, \quad (4)$$

The first term in the right-hand side includes the heating by the shock wave. κ_i is the ion thermal conductivity divided by the Boltzmann constant k. Expressions by Braginskii[26] are used for κ_e and κ_i.

Finally, the equation for magnetic field is given by:

$$\frac{\partial B}{\partial t} + v\frac{\partial B}{\partial r} = -\frac{B}{r}\frac{\partial}{\partial r}(rv) + \frac{1}{r}\frac{\partial}{\partial r}(\frac{c^2}{4\pi}\eta r\frac{\partial B}{\partial r}). \quad (5)$$

A Lagrangian scheme has been adopted to solve Eqs.(1)-(5). The difference equations are written in such a way that Eqs. (1), (3), (4), and (5) are treated implicitly and Eq.(2) explicitly.[23] The spatial grid structure has 30 grid-points and the final grid-point was taken to be at 5 mm with the grid size increasing exponentially from

a minimum size of 20 μm at the center. In this way, we can preserve as much detail as possible near the central region which we are interested in and use the computer CPU time more efficiently.

The plasma outer radius, R_0 (5 mm in calculation) is much larger than the central region (which is typically within 1.5 mm radius). The boundary conditions are

$$T_{e,i} \rightarrow T_0, \quad B \rightarrow B_0, \quad v \rightarrow v_0 \qquad \text{as} \quad r \rightarrow R_0.$$

and at the origin

$$\frac{\partial T_{e,i}}{\partial r} \rightarrow 0, \quad \frac{\partial B}{\partial r} \rightarrow 0, \quad \frac{\partial v}{\partial r} \rightarrow 0 \qquad \text{as} \quad r \rightarrow 0.$$

The initial electron temperature profile is set to be Gaussian with $T_{e,max}$ = 20 eV and $T_{e,min}$ = 3 eV. Then profiles of total ion density, magnetic field, steady-state ionization balance, and electron density are determined by using the local pressure balance. During the time development from the plasma described above, the hydrodynamic code calculates, at each time step, various hydrodynamic parameters, from which electron temperature, electron density and ground state population of Li-like and He-like ions are input to a postprocessor atomic physics code to calculate populations of excited levels and generate line intensities and gains of various transitions in Li-like Al XI.

B. Excited states in the Li-like ion

The level structure considered and relevant transitions in the atomic physics code are shown in Fig. 3. Seventy-seven levels up to the principal quantum number equal

to 12 were included. A population inversion between the 4f and 3d levels is expected for the plasma conditions, in which the electron temperature and density are $T_e \simeq$ 10 eV and $n_e \simeq 5 \times 10^{18}$ cm^{-3}. In this region, levels above n = 5 (n is the principal quantum number) are in local thermal equilibrium with the ground state of He-like ions[27] and their populations are calculated from the Saha-Boltzmann equation. Populations of excited levels from n=2 to n=5 are calculated using the following collisional-radiative model.

We solve the following coupled rate equations:

$$\begin{aligned}\frac{d}{dt}n_{ql} = {} & n_e \sum_{m=l+1}^{k_{max}} (n_{qm}S^{II}_{ml} - n_{ql}S^{I}_{lm}) \\ & + n_e \sum_{m=1}^{l-1} (n_{qm}S^{I}_{ml} - n_{ql}S^{II}_{lm}) \\ & - n_{ql} \sum_{m=1}^{l-1} A_{lm} + \sum_{m=l+1}^{k_{max}} n_{qm}A_{ml} \\ & - n_e n_{ql} S_{ql} + n_{q+1} n_e (\alpha_{ql} + n_e \beta_{ql}), \end{aligned} \tag{6}$$

where n_{ql} denotes the population of an excited level l in the ionization stage q, n_{q+1} the population of the ground state of the ionization stage q+1, S^{I}_{lm} and S^{II}_{lm} the collisional excitation and de-excitation rate between level l and m, respectively, α_{ql} and β_{ql} the radiative and three-body recombination rates, respectively, k_{max} the highest level considered (see Fig. 3), A_{lm} the spontaneous emission rate between level l and m, and S_{ql} the collisional ionization rate from level l.

As discussed by Bates et al.,[28] relaxation of the excited levels is very much more rapid than that of the ground level at the densities presently considered. Thus the left-hand side of Eq.(6) can be set to zero and the calculation of populations of excited

levels for given populations of ground states of adjacent ionization stages becomes an inversion of a matrix whose elements are composed of various rates between the levels:

$$\mathbf{n}_q = -\mathbf{E} \cdot \bar{\bar{\mathbf{C}}}^{-1}, \tag{7}$$

where

$$C_{lm} = \begin{cases} n_e S^{II}_{ml} + A_{ml} & m > l \\ -(n_e \sum_{k=l+1}^{k_{max}} S^{II}_{lk} + \sum_{k=1}^{l-1}(n_e S^{II}_{lk} + A_{lk}) - n_e S_{ql}) & m = l \\ n_e S^{I}_{ml} & m < l \end{cases}$$

$$E_l = n_e n_{q+1}(\alpha_{ql} + n_e \beta_{ql}) + n_e n_{ql} S^{I}_{1l} + \sum_{k=n_{max}+1}^{k_{max}} n_k (n_e S^{II}_{kl} + A_{kl})$$

and $2 < l, m < n_{max}$, where n_{max} is the last level in the collisional-radiative model (see Fig. 3).

The atomic data on various atomic processes used in the solution of the coupled rate equation for populations of excited levels come from a variety of sources. Energy levels and radiative transition rates were taken from the work of Lingård and Nielson.[29] For collisional excitation 2s-nf (n= 4, 5, and 6), works by Petrini were used[30] and for 2p-ns, 2p-np, and 2p-nd (n≥2), rates of Bely and Petrini were taken.[31] The remaining electron collisional excitation rates were estimated from the interpolation formulas by Mewe.[32] An expression for collisional ionization rates from excited states by Post et al.[24] was adopted and the three-body recombination to excited levels and collisional de-excitation rates were estimated by the principle of detailed balance. Only ionization from an excited level to the ground state in the next higher ionization

stage was considered. The radiative recombination rates of Burgess for hydrogen-like ions was used.[33] Dielectronic recombination processes were not included in our calculation because these processes are expected to be negligible compared to three-body recombination processes under the conditions we are interested in.

The plasma is assumed to be optically thin. The 3d-2p transition is the most absorbable because its gA value (g is the statistical weight and A the spontaneous emission rate) is large and the populations of 2p levels is much greater than those of the excited levels. However, even for the 3d-2p transition of Li-like ions in the transverse spectra, the plasma in our experiment is observed to be optically thin in the transverse direction (as discussed in section III).

With populations of excited states calculated as described above, gains at the line center for 4f-3d, 4d-3p, and 4p-3s transitions and line intensities of various transitions shown in Fig. 3 are calculated. The gain per unit length G for a transition between levels l and m is given by

$$G(\lambda_{lm}) = \frac{1}{8\pi c}\frac{\lambda_{lm}^4}{\Delta\lambda} g_l A_{lm}\left[\frac{N_l}{g_l} - \frac{N_m}{g_m}\right] \qquad (\mathrm{cm}^{-1}) \tag{8}$$

where λ_{lm} is the wavelength of the $l - m$ transition and $\Delta\lambda$ is the line width. For the condition of maximum gain presented below, Stark broadening due to the electron impact was smaller than the Doppler broadening by a factor of 2. We have therefore assumed for simplicity that the Doppler-broadening is dominant and $T_i \simeq T_e$ for $T_e \leq 50$ eV throughout the gain calculation.

After the calculation of gains and line intensities as a function of space and time, the axial and transverse spectra for comparisons with experimental data were gen-

erated by integrating the intensity of each line over the spatial region viewed by the axial and transverse spectrometer, respectively and then over time. The amplification by stimulated emission, $(e^{GL}-1)/GL$, in the axial spectrum was taken into account. L is the plasma length which was taken to be 1 cm, as observed in the previous experiment.[34]

III. Experimental results and their comparison with calculation

The experimental set-up is shown in Fig. 4. A CO_2 laser($\sim$ 500J) is focused onto an aluminum or silicon target and creates a highly ionized plasma column confined in a strong axial magnetic field. The maximum laser power density on target is 2×10^{13} W/cm^2. A composite blade made from a sandwich of aluminum and stainless steel (or silicon and titanium for silicon targets) is attached perpendicularly to the target surface (see Fig. 5). We believe that the blade helps to create a more uniform plasma in the axial direction and provides additional cooling by additional radiation losses from the stainless steel or titanium. The plasma is viewed in both axial and transverse directions by multichannel soft x-ray spectrometers,[35] which produce time-integrated spectra.

Theoretical radial profiles of the electron temperature, the electron density, and the gain at the time when the gain reaches its maximum in Li-like Al XI are shown in Fig. 6a. The FWHM (full width at half maximum) of laser pulse was 50 ns, and iron was included as an impurity to provide additional cooling. The center of the

plasma is heated directly by laser and a shock wave is generated which transports ions away from the central hot region, producing favorable conditions for the gain at 1-1.5 mm off-axis. Figure 6b shows the theoretical time history of the gain for the 4f-3d transitions at a radial position 1.2 mm off-axis. The gain peaks at 87 ns from the beginning of the laser pulse and has a duration of about 20 ns in this particular run. The double pulse structure is explained as follows. During the laser pulse He-like ions created in the central hot region diffuse into the region which is 1.2 mm away from the center and still cold. Here they recombine into Li-like ions and produce the first population inversion. As the laser continues to heat plasma, this off-axis region is heated and gain disappears. High gain, however, occurs again at about 90 ns from the beginning of the CO_2 laser pulse as the temperature and density conditions are more appropriate.

Figure 7 shows experimental transverse spectra along with theoretically calculated transverse spectra for comparison. In the spectral region of 140 - 170 Å, line ratios between 141.6, 150.3, and 154.7 Å in the experimental spectra(Fig. 7c) are in a good agreement with those predicted theoretically(Fig. 7d). Note that in Fig. 7c the line intensity ratio of the third order of the 52.3 and 52.45 Å lines, which make up the 3d-2p transition doublet, is 2:1. Considering the fact that the ratio of gA values of this doublet is 2:1 and this transition is the most absorbable, this observation indicates that the plasma is optically thin in the transverse direction for the transitions shown in Fig. 3. This is important as it permits the Al XI 52.4 Å line to depopulate efficiently the 3d level and generate a population inversion. Also, in the wavelength region of 30 - 60 Å(Fig. 7a and 7b), a reasonable agreement between experimen-

tal and theoretical spectra is observed except for the 39.2 Å line, 4f-2p transition. This discrepancy may be due to a change of sensitivity of the detector in the short wavelength region.

The axial emission is imaged by a grazing-incidence mirror onto the entrance slit of a multichannel soft x-ray spectrometer as shown in Fig. 4. The mirror is constructed by bending a glass strip and so, consequently, the optical quality of the system is not ideal. However, a transverse scan of the axial spectrometer enables us to view different ~ 200 μm wide plasma regions. Hence, by changing the transverse position of the axial spectrometer, we are able to adjust the spectrometer to view the region with high gain (we refer to this region as the gain region) or the region with little or no gain (we refer to this region as the non-gain region). On the spectrum recorded from the gain region, we expect to see the amplification of the potential lasing line by stimulated emission. This effect was clearly shown in the work on H-like CVI where extensive observations of absolute intensity and measurements of absolute divergence were the primary evidence for lasing.[6]

Figures 8a and 8c show the spectra recorded by the axial spectrometer at the two different transverse positions of the spectrometer. At one position the intensity of the Al XI 154 Å is significantly increased whereas intensities of other transitions remain almost constant. The ratio of the line intensity of the Al XI 154 Å (4f-3d) to that of the Al XI 141 Å (4p-3s) is three times higher in the gain-region spectrum (Fig. 8a) than in the non-gain-region spectrum (Fig. 8c). Gain-region and non-gain-region spectra including the effect of stimulated emission were generated theoretically by

changing the spatial region over which the intensity of each line was integrated. The computer code models a 1 cm long, cylindrically symmetric plasma, and predicts an annulus gain region approximately 100 μm wide (see Fig. 6). In the experiment the axial spectrometer views a rectangular plasma region $\sim$ 200 μm wide. For the calculated gain-region spectrum, a 200 μm $\times$ 2 mm region of the computer-generated plasma was chosen to include the high gain region and the intensity of each line was integrated spatially over that region and then over time. For the non-gain-region spectrum, the integration region did not include the gain region. As observed in the experimental spectra, the ratio of the 154 Å to 141 Å line intensity is about three times larger in the calculated gain-region spectrum (Fig. 8b) than in the calculated non-gain-region spectrum (Fig. 8d) for the model plasma which has a gain-length product of GL = 3.7. The difference of a factor of 1.7 in the ratio of line intensity of 154 Å to 141 Å between experimental and theoretical spectra could be due to the variation of spectrometer detector sensitivity with wavelength, which has, of course, no effect on present results for relative values of line intensities for the gain and the non-gain region.

Comparison of the axial spectrum in the spectral region of 30 - 60 Å between experiment and calculation is shown in Fig. 9. The experimental spectra, Figs. 9a and 9b, corresponds to the non-gain region and the gain region spectra, respectively. Theoretical spectra were produced by integrating each line over the non-gain region (Fig. 9c) and the gain region (Fig. 9d), as in Fig. 8. Estimation from Eq. (8) shows that at conditions of $T_e \simeq$ 5.0 and $n_e \simeq 3 \times 10^{18}$ cm^{-3} the optical depth of the 52.3 Å resonance line is about 300 μm, which is quite small compared to the axial length

of the plasma, 1 cm. Because of the strong self-absorption of the 52.3 Å resonance line in the axial direction, comparisons involving the 52.3 Å line are of limited value since the present code does not account for opacity. There is, however, one interesting observation that the ratio of intensities of the 48.3 Å line (3p-2s transition) to 54.4 Å line (3s-2p transition) changes from 6.5 in the non-gain region (Fig. 9c) to 2.5 in the gain region (Fig. 9d). This trend can also be seen in experimental spectra (Figs. 9a and 9b). The ratio of the 48.3 Å line to the 54.4 Å line in Fig. 9a is 6.0 and that in Fig. 9b is 4.2. This indicates that the population of the 3p level relative to that of the 3s level in the gain region is lower than it is in the non-gain region. We believe that the reason is that the temperature of the gain region is $\sim$ 5 eV as seen in Fig. 6a and at such temperatures the de-excitation process between 3p and 3s becomes dominant over the excitation process, resulting in an decrease in the 3p level population. Another observation is that, in general, line intensities in Figs. 9b and 9d (the gain-region) is about a third of those in Figs. 9a and 9c (the non-gain-region). This is consistent with an off-axis gain region where the ion densities of He- and Li-like ions are lower than those near on-axis.

A convenient way of showing the amplification of the 4f-3d transition is to measure the line intensity of this transition relative to that of the 4p-3s transition. This comparison, being based on lines in the same ion from upper levels with the same principal quantum number, is independent of uncertainties in the exact spatial distribution of different kinds of ions viewed by the spectrometer. The experimentally observed change in the ratio of the 154 Å to 141 Å line intensities with respect to the transverse position of the axial spectrometer is shown in Fig. 10a, along with com-

putational results. The computations were performed for two plasma conditions with peak gain-length products GL=3.7 and 1.6, respectively. These two conditions were obtained by changing the amount of impurity, iron in our case, while maintaining a constant laser input energy. The additional cooling due to an effective iron concentration of 7 % at $n_e \simeq 4 \times 10^{18} cm^{-3}$ was modeled by using the coronal data[24] with the iron concentration set to 0.7 %(see section IIA). This resulted in a peak gain-length product of GL = 3.7. With an effective iron concentration of 5 % (i.e., 0.5 % used in the code) the gain-length product was GL = 1.6. Experimentally impurities are provided by the interaction of plasma with the composite blade of aluminum and stainless steel. It can be seen that there is a good agreement between the shape of the curves for GL=3.7 and the experimental data.

Similar experiments have been performed with Si XII. In this case the 4f-3d gain transition is at 129 Å and the neighboring 4d-3p and 4p-3s transitions at 126 Å and 119 Å, respectively. The target configuration was similar to Fig. 5 but with a silicon disc and a silicon/titanium composite blade. Since the Si XII ionization potential (523 eV) is higher than that of Al XI(442 eV) and the gain wavelength is shorter, it is expected to be more difficult to generate gain in Si XII than in Al XI. Preliminary results are shown in Fig. 10b where the relative intensity of the 129 Å line compared to the 126 Å and 119 Å lines is shown. The peak in the intensity ratios is a clear indication of gain-length product, GL, of order 1-2 and we expect that with further optimization of experimental conditions higher values of gain will be obtained.

IV. Summary and future plan

We have demonstrated the amplification of 154 Å radiation in Al XI and 129 Å radiation in Si XII for transitions between the 4f and 3d level in a CO_2 laser-produced recombining plasma confined in a strong axial magnetic field. The maximum gain-length products observed are GL $\sim$ 3-4 for 154 Å in Al XI and GL $\sim$ 1-2 for 129 Å in Si XII.

A one-dimensional hydrodynamic code with a postprocessor atomic physics code was used to simulate the experiment. It is shown that the theoretical spectra are in good agreement with experimental data, even though there are several assumptions in the simulation that simplifies the real situation: a cylindrically symmetric plasma, uniform distribution of impurities, and approximation to the energy loss rate of the impurity in a transient, high electron density plasma by scaling steady-state coronal cooling data.

In terms of increasing the power level of the present soft x-ray laser, a large increase in brightness is potentially possible if a cavity formed by two soft x-ray mirrors is applied to a high gain medium. Soft x-ray mirrors with reflectivities in excess of 40 % at 182 Å have recently become available and a cavity formed by two such mirrors combined with a gain medium of gain-length product GL > 3 should oscillate, provided the gain duration is sufficient for several round trips of light between the mirrors ($\geq$ 10 nanoseconds). A 120% increase in stimulated emission was observed in early experiments using one mirror of 12% reflectivity in a double pass configuration[2,36] but mirror alignment posed severe difficulties. A new experimental set-up to

overcome these problems has been constructed and cavity experiments are planned for the near future.

Acknowledgements

We would like to thank H. Furth for support and stimulating discussion. We would also like to acknowledge help from L. Meixler and technical assistance from A. Schuessler and S. Cranmer. This work was made possible by financial support from the U.S. Department of Energy, Advanced Energy Projects of Basic Energy Sciences, the U.S. Air Force Office of Scientific Research, and NRL/SDIO.

References

[*] Also Mechanical and Aerospace Engineering Department of Princeton University.

[1]D. L. Matthews, P. L. Hagelstein, M. D. Rosen, M. J. Eckart, N. M. Ceglio, A. U. Hazi, H. Medecki, B. J. MacGowan, J. E. Trebes, B. L. Whitten, E. M. Camphell, C. W. Hatcher, A. M. Hawryluk, R. L. Kauffman, L. D. Pleasance, G. Rambach, J. H. Scofield, G. Stone, and T. A. Weaver, Phys. Rev. Lett. **54**, 110 (1985).

[2]S. Suckewer, C. H. Skinner, H. Milchberg, C. Keane, and D. Voorhees, Phys. Rev. Lett. **55**, 1753 (1985).

[3]B. J. MacGowan, S. Maxon, P. L. Hagelstein, C. J. Keane, R. A. London, D. L. Matthews, M. D. Rosen, J. H. Scofield, and D. A. Walan, Phys. Rev. Lett. **59**, 2157(1987).

[4]D. Matthews, M. Rosen, S. Brown, N. Ceglio, D. Eder, A. Hawryluk, C. Keane, R. London, B. MacGowan, S. Maxon, D. Nilson, J. Scofield, and J. Trebes, J. Opt. Soc. Am. B **4**, 575 (1987).

[5]P. Jaeglé, G. Jamelot, A. Carillon, A. Klisnick, A. Sureau, and H. Guennou, J. Opt. Soc. Am. B **4**, 563 (1987) and references therein.

[6]S. Suckewer, C. H. Skinner, D. Kim, E. Valeo, D. Voorhees, and A. Wouters, Phys. Rev. Lett. **57**, 1004 (1986).

[7]C. Chenais-Popovics, R. Corbett, C. J. Hooker, M. H. Key, G. P. Kiehn, L. S. Lewis, G. J. Pert, C. Regan, S. J. Rose, S. Sadaat, R. Smith, T. Tomie, and O. Willi,

Phys. Rev. Lett. 59, 2161(1987).

[8]H. C. Kapteyn, R. W. Lee, and R. W. Falcone, Phys. Rev. Lett. 57, 2939(1986).

[9]M. H. Sher, J. J. Macklin, J. F. Young, and S. E. Harris, Opt. Lett. 12, 891(1987).

[10]T. N. Lee, E. A. McLean, and R. C. Elton, Phys. Rev. Lett. 59, 1185(1987).

[11]W. T. Silfvast, O. R. Wood II, J. J. Macklin and H. Lundberg, in *Laser Techniques in the Extreme Ultraviolet*, edited by S. E. Harris and T. B. Lucatorto. AIP Conference Proceedings No. 119 (American Institute of Physics, New York, 1984), p.427.

[12]C. W. Clark, M. G. Littman, R. Miles, T. J. McIlrath, C. H. Skinner, S. Suckewer, and E. Valeo, J. Opt. Soc. Am. B 3, 371 (1986).

[13]M. Duguay and A. Rentzepis, Appl. Phys. Lett. 10, 350(1967).

[14]E. J. McGuire, Phys. Rev. Lett. 35, 844(1975).

[15]P. Jaeglé and M. Key; private communication.

[16]S. Suckewer, C. Keane, H. Milchberg, C.H. Skinner, and D. Voorhees, in *Laser Techniques in the Extreme Ultraviolet*, edited by S. E. Harris and T. B. Lucatorto. AIP Conference Proceedings No. 119 (American Institute of Physics, New York, 1984), p.55.

[17]H. Milchberg, J. L. Schwob, C. H. Skinner, S. Suckewer, and D. Voorhees, in *Laser Techniques in the Extreme Ultraviolet*, edited by S. E. Harris and T. B. Lucatorto.

AIP Conference Proceedings No. 119 (American Institute of Physics, New York, 1984), p.379.

[18]E. Valeo, C. Keane, and R. M. Kulsrud, Bull. Am. Phys. Soc. **30**, 1600 (1985).

[19]P. G. Burkhalter, M. J. Herbst, D. Duston, J. Gardner, M. Emery, R. R. Whitlok, J. Grun, J. P. Apruzese, and J. Davis, Phys. Fluids **26**, 3650(1983) and references therein.

[20]R. W. P. McWhirter, in *Plasma Diagnostic Techniques*, edited by R. H. Huddlestone and S. L. Leonard (Academic Press, New York, 1965) p. 205.

[21]H. P. Summers, Mon. Not. R. Astron. Soc. **169**, 663 (1974); Rutherford-Appleton Laboratory Report No. IM367 (1974).

[22]H. P. Summers, Comments At. Mol. Phys. **14**, 147 (1984).

[23]R. D. Richtmyer and K. W. Morton, *Difference Methods for Initial Value Problems* (Interscience, New York, 1957).

[24]D. E. Post, R. V. Jensen, C. B. Tarter, W. H. Grasberger, and W. A. Lokke, At. Data Nucl. Data Tables **20**, 397 (1977).

[25]C. Keane and C. H. Skinner, Phys. Rev. A **33**, 4179 (1986).

[26]S. I. Braginskii, in *Reviews of Plasma Physics*, edited by M. A. Leontovich (Consultants Bureau, New York, 1965), vol. 1, p.205.

[27]R. Wilson, J. Quant. Spectrosc. Radiat. Transfer **2**, 477 (1962).

[28]D. R. Bates, F. R. S., A. E. Kingston and R. W. P. McWhirter, Proc. R. Soc. **A267**, 297 (1962).

[29]A. Lingård and S. E. Nielson, At. Data Nucl. Data Tables **19**, 533 (1977).

[30]D. Petrini, Astron. & Astrophys. **17**, 410 (1972).

[31]O. Bely and D. Petrini, Astron. & Astrophys. **6**, 318 (1970).

[32]R. Mewe, Astron. & Astrophys. **20**, 215 (1972).

[33]A. Burgess, Mem. R. Astr. Soc. **69**, 1 (1965).

[34]C. H. Skinner, C. Keane, H. Milchberg, S. Suckewer, and D. Voorhees, in *Laser Techniques in the Extreme Ultraviolet*, edited by S. E. Harris and T. B. Lucatorto. AIP Conference Proceedings No. 119 (American Institute of Physics, New York, 1984), p.372.

[35]J. L. Schwob, A. Wouters, and S. Suckewer, Rev. Sci. Instrum. **58**, 1601(1987).

[36]C. Keane, C. H. Nam, L. Meixler, H. Milchberg, C. H. Skinner, S. Suckewer, and D. Voorhees, Rev. Sci. Instrum. **57**, 1296 (1986).

Figures

FIG. 1. The maximum gain and its position versus the diffusion coefficient with laser input energy and amount of impurity (iron) kept the same.

•: the maximum gain of the 4f-3d transition in Li-like Al XI

○: the radial position where the maximum gain occurs

Lines are drawn between points as a visual aid.

FIG. 2. The variation of the reduction factor, $1 - n_e S_{lm}^{II}/A_{lm}$, of the radiative cooling rate per ion per electron with respect to the electron temperature at given electron densities. In low electron densities (solid dot points), the factor becomes close to unity but in high electron densities (open circles) and low electron temperature $\Delta n = 0$ collisional de-excitation rates dominate $\Delta n = 0$ radiative transition rates, resulting in the reduction in the cooling rate. This calculation was done for iron using the average-ion model used by Post et al.[24] Lines are drawn as a visual aid.

FIG. 3. Grotrian diagram of Li-like Al.

FIG. 4. Experimental set-up.

FIG. 5. An aluminum disc target geometry with a 0.8 x 2 mm vertical slot and an aluminum/stainless steel composite blade attached perpendicular to the target surface.

FIG. 6. (a)Calculated radial profiles of electron density, electron temperature, and gain for the 4f-3d transition(154 A) at the time of maximum gain in Li-like Al XI.

(b)The time history of the gain for the 4f-3d transition in Li-like Al XI at a radial position 1.2 mm off-axis.

FIG. 7. (a) and (c) are plasma emissions recorded by the transverse spectrometer in the spectral range of 30 - 60 Å and 140 - 170 Å, respectively; (b) and (d) are calculated transverse emission spectra in those spectral ranges. The line widths in the theoretical spectra do not have any physical meaning.

FIG. 8. Axial spectra in the spectral region of 140 - 170 Å: (a) and (c) were recorded by the axial spectrometer for the gain and the non-gain region, respectively; (b) and (d) are calculated time-integrated axial spectra over the gain region and the non-gain region, respectively.

FIG. 9. Axial spectra in the spectral region of 30 - 60 Å: (a) and (b) were recorded by the axial spectrometer for the non-gain and gain region, respectively. (c) and (d) are calculated time-integrated axial spectra over the non-gain region and the gain region, respectively.

FIG. 10. (a) Observed and predicted line intensity ratio versus horizontal position of the axial spectrometer showing the rise in relative intensity of the Al XI 4f-3d transition at 154.7 Å in the region of the plasma with gain.

•: experimental data,

o: modeling with peak gain-length product, GL = 1.6,

+: modeling with peak gain-length product, GL = 3.7

(b)The line ratios of SiXII 129 Å to 119 Å and SiXII 129 Å to 126 Å are shown as a function of the transverse position of the axial spectrometer.

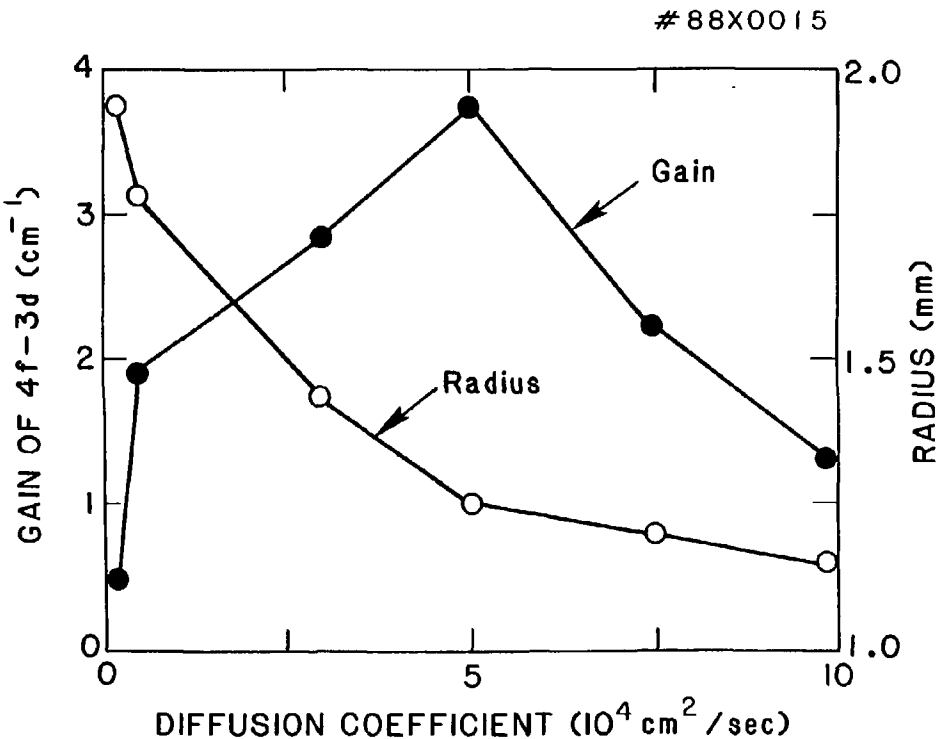
#88X0015
GAIN OF 4f-3d (cm⁻¹)
RADIUS (mm)
DIFFUSION COEFFICIENT (10⁴ cm² / sec)
Gain
Radius
0
1
2
3
4
5
10
1.0
1.5
2.0

Figure 1

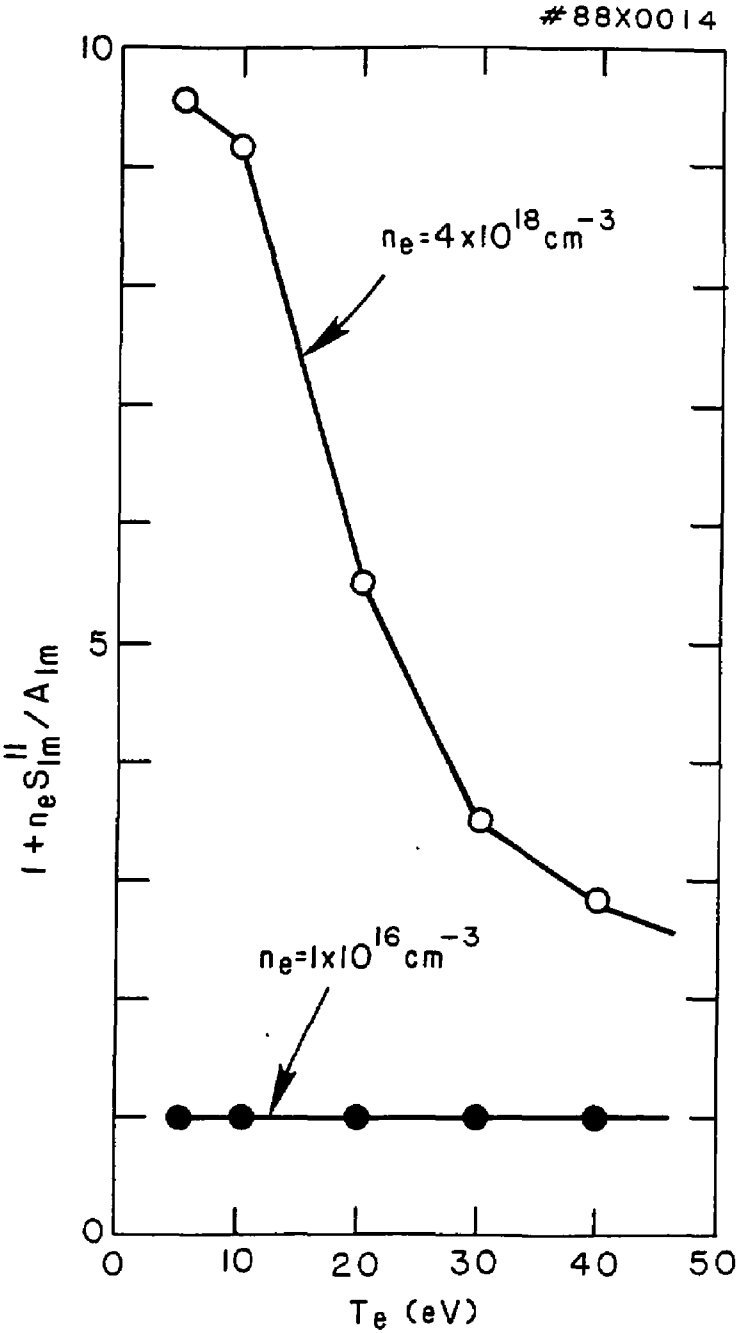
#88X0014
10
5
0
0
10
20
30
40
50
$n_e=4\times10^{18}cm^{-3}$
$n_e=1\times10^{16}cm^{-3}$
$1+n_eS^{II}_{lm}/A_{lm}$
T_e (eV)

Figure 2

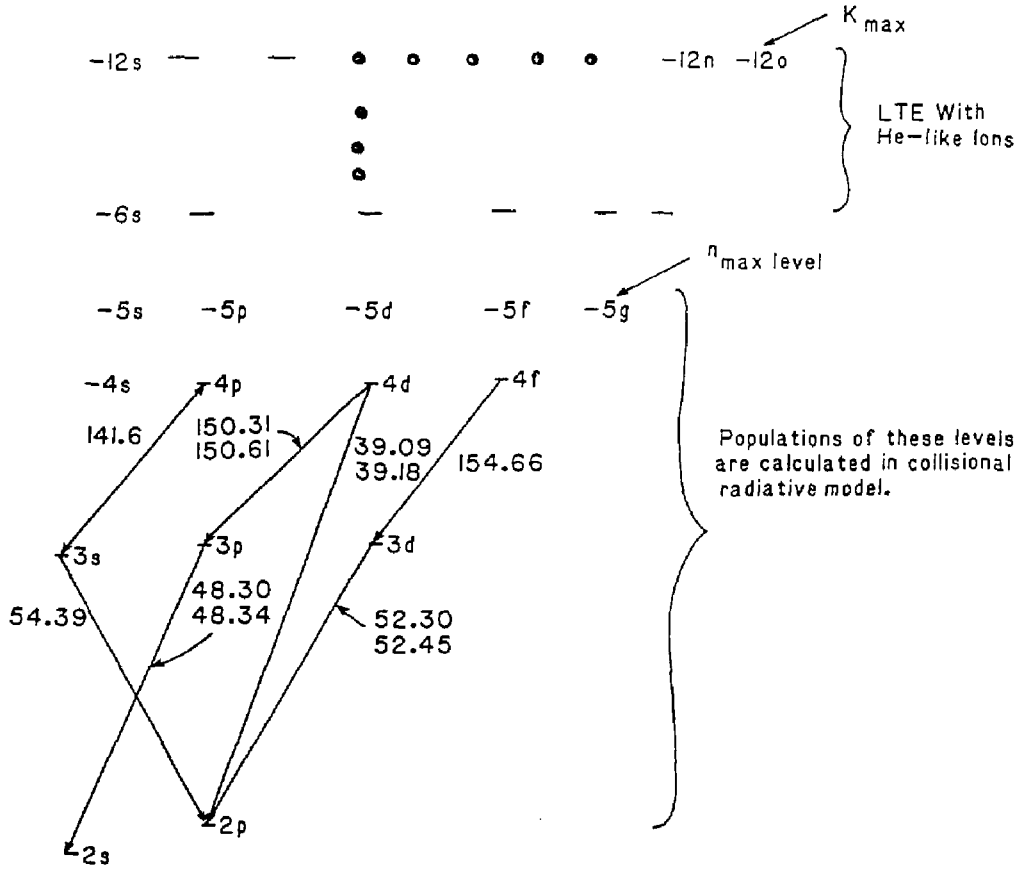
K max
-12s
-12n
-12o
LTE With
He-like Ions
-6s
n max level
-5s
-5p
-5d
-5f
-5g
-4s
4p
4d
4f
141.6
150.31
150.61
39.09
39.18
154.66
Populations of these levels
are calculated in collisional
radiative model.
3s
3p
3d
48.30
48.34
54.39
52.30
52.45
2p
2s

Figure 3

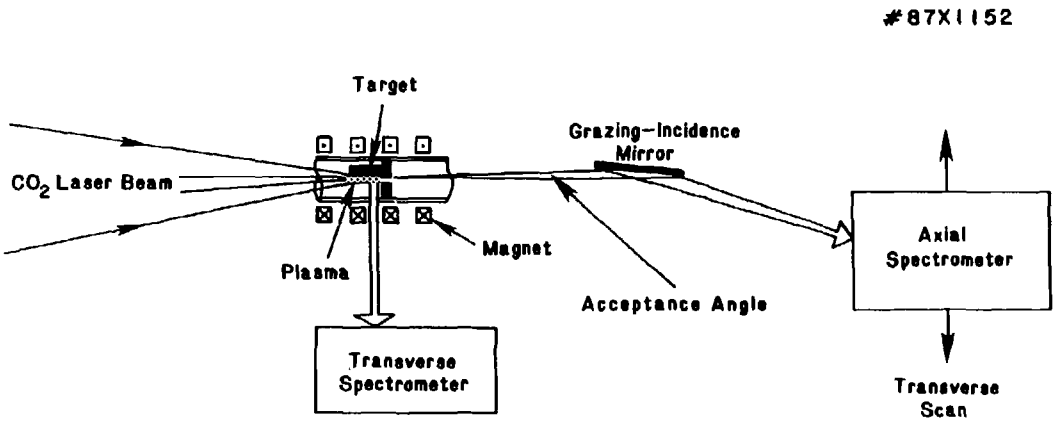
#87X1152
Target
CO_2 Laser Beam
Grazing-Incidence Mirror
Axial Spectrometer
Plasma
Magnet
Acceptance Angle
Transverse Spectrometer
Transverse Scan

Figure 4

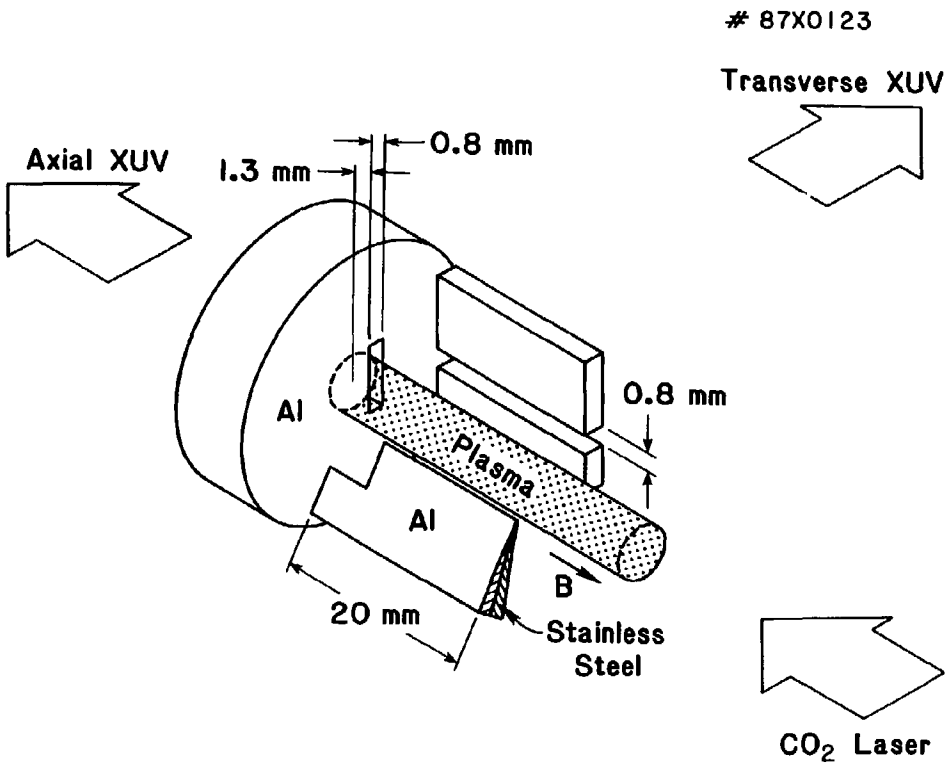
87X0123
Transverse XUV
Axial XUV
1.3 mm
0.8 mm
Al
0.8 mm
Plasma
Al
B
20 mm
Stainless Steel
CO_2 Laser

Figure 5

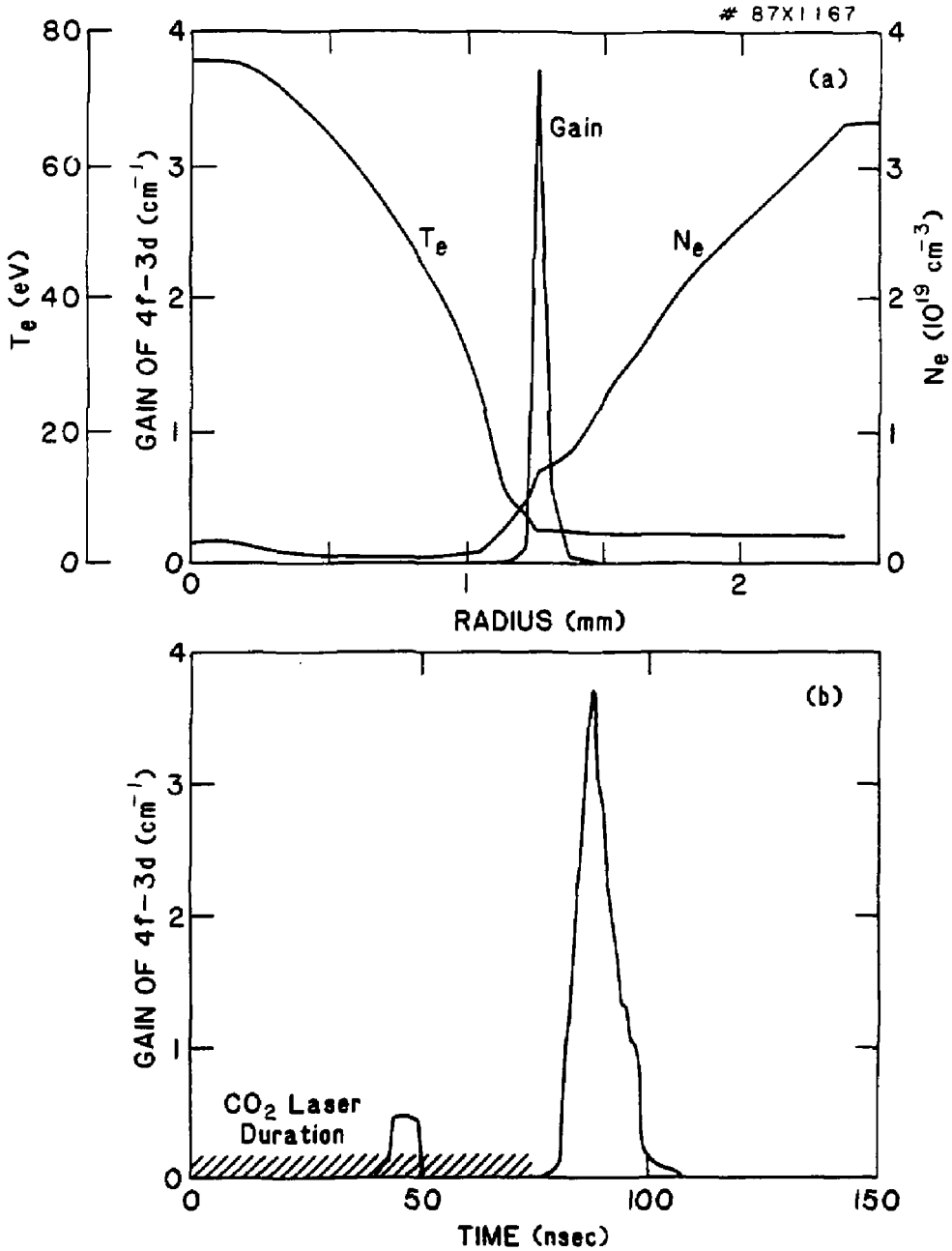
87X1167
(a)
Gain
T_e
N_e
T_e (eV)
GAIN OF 4f-3d (cm^{-1})
N_e (10^{19} cm^{-3})
RADIUS (mm)
(b)
CO_2 Laser Duration
TIME (nsec)

Figure 6

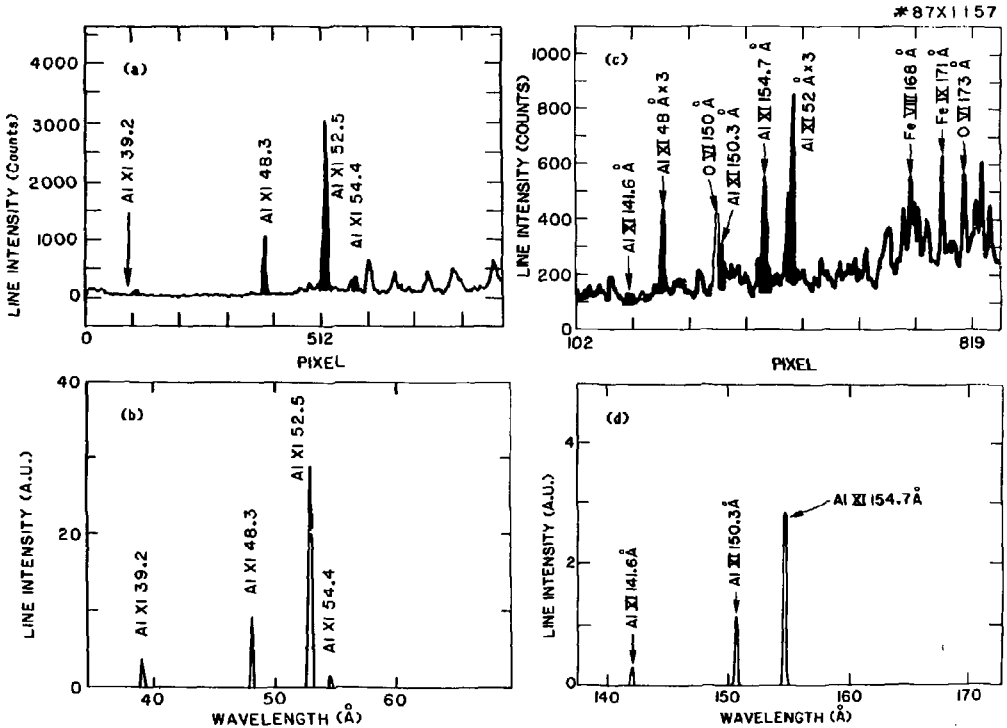
#87X1157
(a)
LINE INTENSITY (Counts)
Al XI 39.2
Al XI 48.3
Al XI 52.5
Al XI 54.4
PIXEL
(c)
LINE INTENSITY (COUNTS)
Al XI 141.6 Å
Al XI 48 Å x3
O VII 150 Å
Al XI 150.3 Å
Al XI 154.7 Å
Al XI 52 Å x3
Fe VIII 168 Å
Fe IX 171 Å
O VI 173 Å
PIXEL
(b)
LINE INTENSITY (A.U.)
Al XI 39.2
Al XI 48.3
Al XI 52.5
Al XI 54.4
WAVELENGTH (Å)
(d)
LINE INTENSITY (A.U.)
Al XI 141.6Å
Al XI 150.3Å
Al XI 154.7Å
WAVELENGTH (Å)

Figure 7

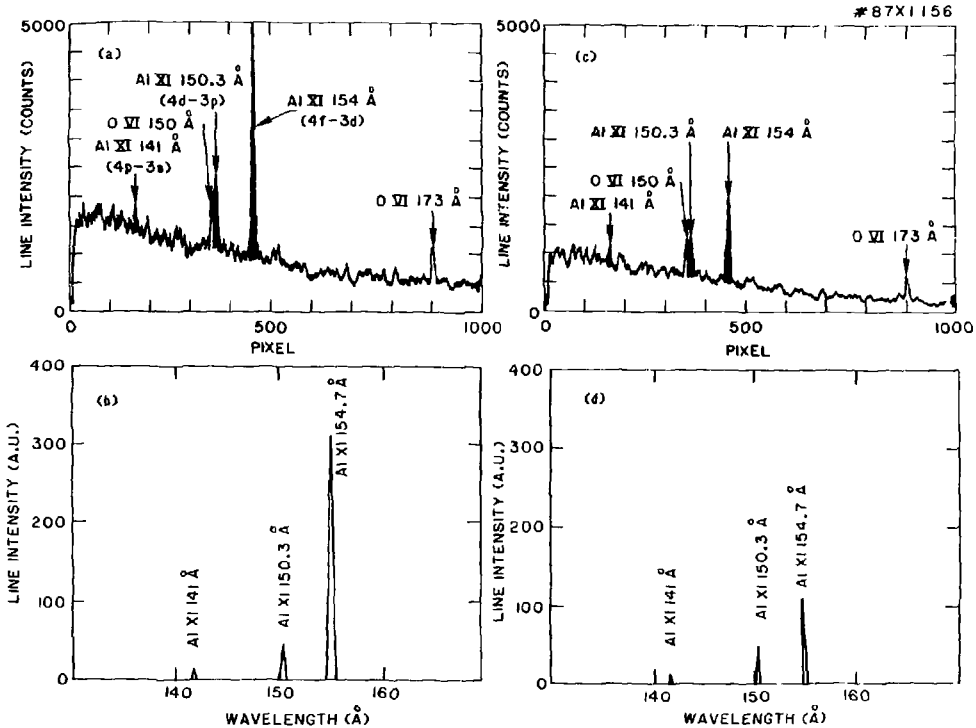
#87X1156
(a)
Al XI 150.3 Å
(4d-3p)
Al XI 154 Å
(4f-3d)
O VI 150 Å
Al XI 141 Å
(4p-3s)
O VI 173 Å
LINE INTENSITY (COUNTS)
PIXEL
(c)
Al XI 150.3 Å
Al XI 154 Å
O VI 150 Å
Al XI 141 Å
O VI 173 Å
(b)
Al XI 141 Å
Al XI 150.3 Å
Al XI 154.7 Å
LINE INTENSITY (A.U.)
WAVELENGTH (Å)
(d)

Figure 8

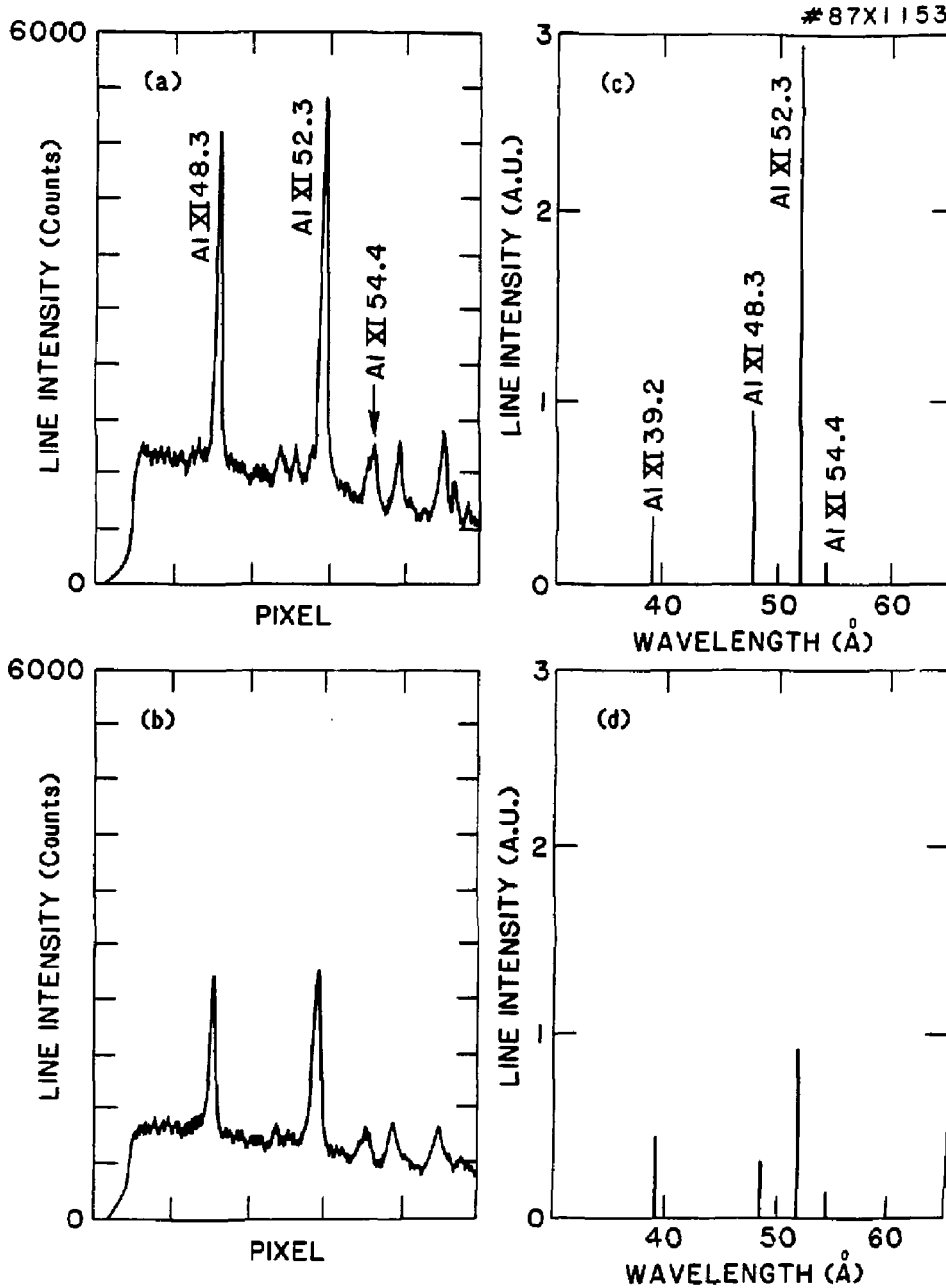
#87X1153
(a)
(b)
(c)
(d)
6000
0
LINE INTENSITY (Counts)
PIXEL
Al XI 48.3
Al XI 52.3
Al XI 54.4
3
2
1
0
LINE INTENSITY (A.U.)
Al XI 39.2
40
50
60
WAVELENGTH (Å)

Figure 9

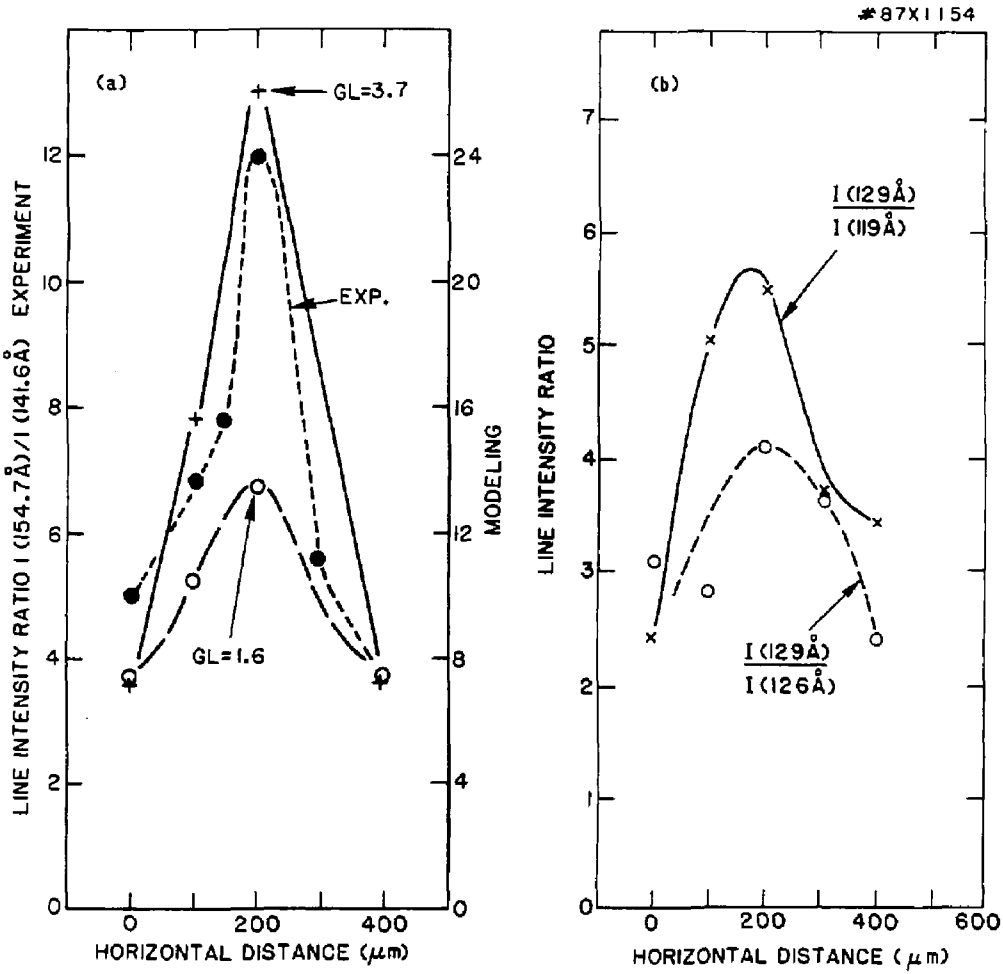
#87X1154
(a)
GL=3.7
EXP.
GL=1.6
LINE INTENSITY RATIO I (154.7Å)/I (141.6Å) EXPERIMENT
MODELING
HORIZONTAL DISTANCE (μm)
(b)
I (129Å) / I (119Å)
I (129Å) / I (126Å)
LINE INTENSITY RATIO
HORIZONTAL DISTANCE (μm)

Figure 10

EXTERNAL DISTRIBUTION IN ADDITION TO UC-20

Dr. Frank J. Paoloni, Univ of Wollongong, AUSTRALIA
Prof. M.H. Brennan, Univ Sydney, AUSTRALIA
Plasma Research Lab., Australian Nat. Univ., AUSTRALIA
Prof. I.R. Jones, Flinders Univ., AUSTRALIA
Prof. F. Cap, Inst Theo Phys, AUSTRIA
Prof. M. Heindler, Institut fur Theoretische Physik, AUSTRIA
M. Goossens, Astronomisch Instituut, BELGIUM
Ecole Royale Militaire, Lab de Phys Plasmas, BELGIUM
Commission-Eurogean, Dg-XII Fusion Prog, BELGIUM
Prof. R. Boucique, Laboratorium voor Natuurkunde, BELGIUM
Dr. P.H. Sakanaka, Instituto Fisica, BRAZIL
Instituto De Pesquisas Especiasi-INPE, BRAZIL
Documents Office, Atomic Energy of Canada Limited, CANADA
Dr. M.P. Bachynski, MPB Technologies, Inc., CANADA
Dr. H.M. Skarsgard, University of Saskatchewan, CANADA
Dr. H. Barnard, University of British Columbia, CANADA
Prof. J. Teichmann, Univ. of Montreal, CANADA
Prof. S.R. Sreenivasan, University of Calgary, CANADA
Prof. Tudor W. Johnston, INRS-Energie, CANADA
Dr. C.R. James, Univ. of Alberta, CANADA
Dr. Peter Lukac, Komenskeho Univ, CZECHOSLOVAKIA
The Librarian, Culham Laboratory, ENGLAND
The Librarian, Rutherford Appleton Laboratory, ENGLAND
Mrs. S.A. Hutchinson, JET Library, ENGLAND
C. Mouttet, Lab. de Physique des Milieux Ionises, FRANCE
J. Radet, CEN/CADARACHE - Bat 506, FRANCE
Univ. of Ioannina, Library of Physics Dept. GREECE
Dr. Tom Mual, Academy Bibliographic Ser., HONG KONG
Preprint Library, Hungarian Academy of Sciences, HUNGARY
Dr. B. Dasgupta, Saha Inst of Nucl. Phys., INDIA
Dr. P. Kaw, Institute for Plasma Research, INDIA
Dr. Philip Rosenau, Israel Inst. Tech, ISRAEL
Librarian, Int'l Ctr Theo Phys, ITALY
Prof. G. Rostagni, Univ Of Padova, ITALY
Miss Clelia De Palo, Assoc EURATOM-ENEA, ITALY
Biblioteca, Instituto di Fisica del Plasma, ITALY
Dr. H. Yamato, Toshiba Res & Dev, JAPAN
Prof. I. Kawakami, Atomic Energy Res. Institute, JAPAN
Prof. Kyoji Nishikawa, Univ of Hiroshima, JAPAN
Direc. Dept. Large Tokamak Res. JAERI, JAPAN
Prof. Soroshi Itoh, Kyushu University, JAPAN
Research Info Center, Nagoya University, JAPAN
Prof. S. Tanaka, Kyoto University, JAPAN
Library, Kyoto University, JAPAN
Prof. Nobuyuki Inoue, University of Tokyo, JAPAN
S. Mori, JAERI, JAPAN
Librarian, Korea Advanced Energy Res. Institute, KOREA
Prof. D.I. Choi, Adv. Inst Sci & Tech, KOREA
Prof. B.S. Liley, University of Waikato, NEW ZEALAND
Institute of Plasma Physics, PEOPLE'S REPUBLIC OF CHINA
Librarian, Institute of Phys., PEOPLE'S REPUBLIC OF CHINA
Library, Tsing Hua University, PEOPLE'S REPUBLIC OF CHINA
Z. Li, Southwest Inst. Physics, PEOPLE'S REPUBLIC OF CHINA
Prof. J.A.C. Cabral, Inst Superior Tecnico, PORTUGAL
Dr. Octavian Petrus, AL I CUZA University, ROMANIA
Dr. Johan de Villiers, Fusion Studies, AEC, SO AFRICA
Prof. M.A. Hellberg, University of Natal, SO AFRICA
C.I.E.M.A.T., Fusion Div. Library, SPAIN
Dr. Lennart Stenflo, University of UMEA, SWEDEN
Library, Royal Inst Tech, SWEDEN
Prof. Hans Wilhelmson, Chalmers Univ Tech, SWEDEN
Centre Phys des Plasmas, Ecole Polytech Fed, SWITZERLAND
Bibliotheek, Fom-Inst Voor Plasma-Fysica, THE NETHERLANDS
Dr. D.D. Ryutov, Siberian Acad Sci, USSR
Dr. G.A. Eliseev, Kurchatov Institute, USSR
Dr. V.A. Glukhikh, Inst Electrophysical Apparatus, USSR
Dr. V.T. Tolok, Inst. Phys. Tech. USSR
Dr. L.M. Kovrizhnykh, Institute Gen. Physics, USSR
Nuclear Res. Establishment, Julich Ltd., W. GERMANY
Bibliothek, Inst. Fur Plasmaforschung, W. GERMANY
Dr. K. Schindler, Ruhr Universitat Bochum, W. GERMANY
ASDEX Reading Rm, IPP/Max-Planck-Institut fur Plasmaphysik, W. GERMANY
Librarian, Max-Planck Institut, W. GERMANY
Prof. R.K. Janev, Inst Phys, YUGOSLAVIA